Published in final edited form as:

Cancer Res. 2018 June 01; 78(11): 3002–3013. doi:10.1158/0008-5472.CAN-17-2433.

Activation of the receptor tyrosine kinase AXL regulates the immune microenvironment in glioblastoma

Hirokazu Sadahiro[1,2,#], **Kyung-Don Kang**[1,#], **Justin T. Gibson**[3], **Mutsuko Minata**[1], **Hai Yu**[1,4], **Junfeng Shi**[5], **Rishi Chhipa**[6], **Zhihong Chen**[7], **Songjian Lu**[8], **Yannick Simoni**[9], **Takuya Furuta**[10], **Hemragul Sabit**[11], **Suojun Zhang**[1,12], **Soniya Bastola**[1], **Shinobu Yamaguchi**[1], **Hebaallah Alsheikh**[1], **Svetlana Komarova**[1], **Jun Wang**[1], **Sung-Hak Kim**[13], **Dolores Hambardzumyan**[7], **Xinghua Lu**[8], **Evan W. Newell**[9], **Biplab DasGupta**[6], **Mitsutoshi Nakada**[11], **L. James Lee**[5], **Burt Nabors**[1], **Lyse A. Norian**[3,14], and **Ichiro Nakano**[1,14,*]

[1]Department of Neurosurgery, University of Alabama at Birmingham, Birmingham, Alabama

[2]Department of Neurosurgery, Yamaguchi University, Yamaguchi, Japan

[3]Department of Nutrition Sciences, University of Alabama at Birmingham, Birmingham, Alabama

[4]Department of Neurosurgery, The First Affiliated Hospital of Xi'an Jiaotong University, Xi'an, China

[5]Department of Chemical and Biomolecular Engineering, The Ohio State University, Columbus, Ohio

[6]Division of Oncology, Cincinnati Children's Hospital Medical Center, Cincinnati, Ohio

[7]Department of Pediatrics, Aflac Cancer and Blood Disorders Center, Children's Healthcare of Atlanta, Emory University School of Medicine, Atlanta, Georgia

[8]Department of Biomedical Informatics, University of Pittsburgh, Pittsburgh, Pennsylvania

[9]Singapore Immunology Network, Agency for Science Technology and Research, Singapore, and the Nanyang Technological University School of Biological Sciences, Singapore

[10]Department of Pathology, Kurume University School of Medicine, Kurume, Japan

[11]Department of Neurosurgery, Division of Neuroscience, Graduate School of Medical Science, Kanazawa University, Kanazawa, Japan

[12]Department of Neurosurgery, Tongji Hospital, Tongji Medical College, Huazhong University of Science and Technology, Wuhan, China

[13]Department of Animal Science, College of Agriculture and Life Sciences, Chonnam National University, Gwangju, Republic of Korea

[14]UAB Comprehensive Cancer Center, University of Alabama at Birmingham, Birmingham, Alabama

[*]Correspondence: Ichiro Nakano, MD, PhD, University of Alabama at Birmingham; Department of Neurosurgery, 1824 6th Avenue South, Wallace Tumor Institute 202, Birmingham, AL 35233, Phone: 614-292-0358, inakano@uabmc.edu.

[#]Equal Contribution

The authors declare no potential conflicts of interest.

Abstract

Glioblastoma (GBM) is a lethal disease with no effective therapies available. We previously observed upregulation of the TAM (Tyro-3, Axl, and Mer) receptor tyrosine kinase family member AXL in mesenchymal GBM and showed that knockdown of AXL induced apoptosis of mesenchymal, but not proneural, glioma sphere cultures (GSCs). In this study, we report that BGB324, a novel small molecule inhibitor of AXL, prolongs the survival of immunocompromised mice bearing GSC-derived mesenchymal GBM-like tumors. We show that protein S (PROS1), a known ligand of other TAM receptors, was secreted by tumor-associated macrophages/microglia and subsequently physically associated with and activated AXL in mesenchymal GSC. PROS1-driven phosphorylation of AXL (pAXL) induced NF-κB activation in mesenchymal GSC, which was inhibited by BGB324 treatment. We also found that treatment of GSC-derived mouse GBM tumors with Nivolumab, a blocking antibody against the immune checkpoint protein PD-1, increased intratumoral macrophages/microglia and activation of AXL. Combinatorial therapy with Nivolumab plus BGB324 effectively prolonged the survival of mice bearing GBM tumors. Clinically, expression of AXL or PROS1 was associated with poor prognosis for GBM patients. Our results suggest that the PROS1-AXL pathway regulates intrinsic mesenchymal signaling as well as the extrinsic immune microenvironment, contributing to the growth of aggressive GBM tumors.

Keywords

glioma stem cell; cancer stem cell; BGB324; PROS1; PDGFRα

Introduction

Glioblastoma (GBM) is among the most lethal of adult cancers. The median survival of patients remains less than two years despite the current available therapies, including surgery, radiation, and chemotherapy; development of more effective therapies is urgently needed.

We have recently reported that increased expression of the receptor tyrosine kinase AXL is significantly correlated with poor prognosis in GBM. Furthermore, we found that AXL expression is elevated in the mesenchymal (MES) GBM subtype (1). AXL, along with TYRO3 and MERTK, belong to the TAM family of kinases, which are activated by the growth arrest-specific protein 6 (GAS6) and protein S (PROS1) ligands. Previous reports have shown that GAS6 binds all three receptors, while PROS1 interacts with TYRO3 and MERTK, but not with AXL (2–4). GAS6-driven AXL signaling is known to have various tumor-promoting effects. For example, acute myeloid leukemia (AML) cells induce bone marrow-derived stromal cells to express and secrete GAS6, which in turn mediates proliferation, survival, and chemoresistance of AXL-expressing AML cells (5). In lung cancers that express a mutant form of the epidermal growth factor receptor (EGFR) associated with acquired resistance to tyrosine kinase inhibitors, expression of both AXL and GAS6 is increased (6). Elucidation of these pro-oncogenic roles of AXL has resulted in increasing interest in AXL as a clinical target. In 2013, a clinical trial for a small molecule AXL inhibitor, BGB324 (also known as R428), was launched for the treatment of colon

cancer (7). More recently, a second clinical trial investigating BGB324 in the AML and non-small cell lung cancer settings has been initiated in the United States (NCT02424617).

In addition to direct effects on tumor cells, in some cancers, AXL also appears to promote immune suppression through transcriptional regulation of the immune checkpoint ligand, PD-L1 (8). Nivolumab and Pembrolizumab were the first two checkpoint inhibitors designed to target the PD-L1 receptor, PD-1. In 2014, both were approved by the Food and Drug Administration (FDA) for the treatment of unresectable and metastatic melanoma (9). In a clinical trial for patients with metastatic melanoma, treatment with Nivolumab alone, or in combination with the cytotoxic T-lymphocyte-associated antigen-4 (CTLA-4) antibody, Ipilimumab, resulted in significantly longer patient survival than did treatment with Ipilimumab alone (10). In the setting of GBM, several preclinical studies investigating immune checkpoint inhibitors have demonstrated that antibodies targeting CTLA-4, PD-1, or PD-L1 produce tumor regression and survival benefit in syngeneic GBM murine models (11,12). Furthermore, combination treatment using an anti-PD-1 mAb and localized radiation therapy increased the survival of mice bearing orthotopic brain tumors (13). Based on these encouraging preclinical data, a phase III clinical trial (NCT02017717) was initiated in 2014 to compare the efficacy of Nivolumab with that of Bevacizumab for the treatment of recurrent GBM. However, this first trial failed to demonstrate Nivolumab efficacy, for reasons that remain unclear. Several additional clinical trials investigating PD-1/PD-L1 checkpoint inhibitors for the treatment of GBM, both as monotherapy, and in combination with other therapies such as radiotherapy (NCT02667587), surgery (NCT02337686), or temozolomide treatment (NCT0261758) are currently underway (14–16).

In this study, we tested the hypothesis that AXL signaling promotes GBM tumor growth through intrinsic mechanisms that regulate survival and growth of glioma stem cells (GSCs) and immune-suppressive extrinsic signals that modify the tumor microenvironment. First, we sought to determine the molecular mechanisms associated with AXL signaling in patient-derived GSCs, both *in vitro*, using GSC-enriched cultures, and *in vivo*, using xenograft models in immunocompromised mice. We then investigated the efficacy of the AXL inhibitor, BGB324, either by monotherapy, using both human GSC xenografts in immunocompromised mice or murine GBM in immunocompetent mice, or in combination with Nivolumab in pre-clinical murine GBM models in immunocompetent mice.

Materials and Methods

Ethics

Experiments were defined to be exempt from requiring consent by the Institutional Review Board (IRB) and Institutional Animal Care and Use Committee (IACUC) protocols of University of Alabama at Birmingham, MD Anderson Cancer Center (MDACC), University of California at Los Angeles (UCLA), and Ohio State University (OSU). Mouse studies were conducted using protocols approved by IACUC and were performed in accordance with NIH guidelines (IRB protocol number: #151013001).

Patient-derived GBM (neuro)sphere cultures

The GBM sphere cultures used in this study were generated at UAB, MDACC, UCLA, and OSU, independently validated by short tandem repeat (STR) analysis. GBM sphere cultures (1,17–19) were maintained in DMEM/F12/Glutamax (Gibco) with epidermal growth factor (EGF, Peprotech), basic fibrous growth factor (bFGF, Peprotech), heparin (Sigma), and B27 (neuroBrew-21 w/o Vitamin A, MACS). EGF, bFGF, and heparin were added twice weekly. The cell lines were cultivated for no longer than 30 passages. Mouse GBM sphere cultures were established as described previously (20) and cultured in the same medium described above. The cell lines were tested negative for mycoplasma contamination.

In vitro AXL and PDGFRα mRNA Detection by Nanochannel Electroporation (NEP) - delivered Molecular Beacon (MB) Probes

AXL MB (Cy5-labeled) and PDGFRα MB (FAM-labeled) were co-delivered into GSCs (GBM157) by 3D Nanochannel electroporation (NEP) chips designed for large-scale uniform and benRign cell transfection (21,22). The cells were seeded as monolayer in 3D silicon NEP chip overnight in 10% FBS, heparin-free glioma cell culture medium before the NEP-based transfection to ensure a tight contact between cells and nanochannel array. Before the nano-electroporation for intracellular delivery of MBs, the MB solution was prepared in the optimal concentration from 200 nM to 500 nM and then pipetted in the reservoir on the bottom gold-coated electrode slide with 500uL to 1mL volume. The MBs were then NEP-injected into the single glioma clones on the 3D NEP chip surface by applying an electric field pulse with conditions of 150–200 Voltage, 20 –30 ms duration, across the nanochannel arrays. After 1-hour incubator, MB hybridization with the specific target mRNA biomarker gradually occurred, and the marker expression was then quantified by fluorescence intensity, which came from the hybridized MB fluorescence emission, as the original hairpin-loop structure was open, separating fluorescent dye from the quencher. Fluorescence microscope system (Eclipse Ti-E, Nikon) equipped with motorized stage and EMCCD camera (Evolve, Photometrics) was used for imaging. Quantitative analysis of fluorescence intensity was through image processing using the software NIS- Elements Advanced Research. All molecular beacon probes were purchased from Sigma-Aldrich, St. Louis, MO.

Measurement of the extracellular acidification rate (ECAR) and O_2 consumption rate (OCR)

For ECAR and OCR, 2×10^4 cells were seeded in 96-well Seahorse plates in DMEM with 10% FCS, 16h before assay and ECAR and OCR were analyzed using the XF^{e}96-Analyzer (Seahorse Biosciences). Cells were equilibrated with DMEM lacking bicarbonate at 37°C for 1h in a custom incubator without CO_2. OCR and ECAR were measured at baseline and following the addition of reagents (oligomycin: 3 μM, FCCP: 3 μM and antimycin: 10 μM as final concentrations) for indicated times.

CD11b MACS enrichment and Flow cytometry

Brain tumors were removed from GBM sphere-derived xenograft mice. The tumors were homogenized and dissociated with collagenase (ThermoFisher) at 37 °C for 30 min. Cells were resuspended in autoMACS Rinsing Solution [5% MACS bovine serum albumin (BSA)

stock solution] containing CD11b microbeads (Miltenyl Biotec) and incubated at 4 °C for 15 min. Additionally, CD11b-FITC (Miltenyl Biotec) was added to the rinsing solution at 4 °C for 5 min. The solution was clarified by centrifugation, the supernatant was discarded, and cell pellets were resuspended in rinsing solution. Samples were then sorted using magnetic separation, followed by flow cytometry with Attune NxT (Life Technology). Isolated cells were cultured in RMPI-1640 medium without serum for 48 hours, and the supernatant was collected to serve as MG/Mø conditioned medium.

CyTOF staining and data analysis

CyTOF was carried out as previously described (23). Briefly, GBM tumors were excised and digested in collagenase/hyaluronidase and DNase I and dissociated by gentleMACs. Prior to surface staining, cells were stained with Cisplatin (viability marker). Cells were then stained and analyzed by CyTOF. The CyTOF data were exported in a conventional flow-cytometry file (.fcs) format and normalized using previously described software (24).

GEO accession number

The accession number of GEO dataset in this study is GSE67089.

Statistical analyses

Statistical analyses were performed using Prism 7.01 software. All data are presented as the mean ± standard deviation (SD). *P*-values less than 0.05 were considered statistically significant. Statistical differences between two groups were evaluated using two-tailed *t*-tests. Statistically significant differences in Kaplan-Meier survival curves were determined by log-rank analysis. A statistical correlation was performed to calculate the regression R^2 value and Spearman's correlation coefficient.

Results

Downregulation of PDGFRα drives AXL expression accompanied by increased glycolysis in GSCs

We previously reported that AXL is highly expressed in MES GBM. To further determine the magnitude of increased AXL expression in MES tumor cells, we used genome-wide transcriptome microarray analysis (GSE67089) to compare expression of 49 different receptor tyrosine kinases (RTKs) between proneural (PN) and MES GSCs (19) and between untreated PN GSCs and the radiation therapy-treated (RT) counterparts that gained MES signature (25) (Fig. 1A and Supplementary Fig. S1A). Our analysis confirmed that AXL is highly expressed in MES and RT-PN GSCs, whereas expression of PDGFRα is low in MES and RT-PN GSCs. The negative correlation between expression of PDGFRα and AXL mRNA was also observed in PDGF-driven mouse GBM models (Fig. 1B). Western blot analysis of lysates from GSCs and U87 cells also showed a negative correlation between expression of PDGFRα and AXL (Fig. 1C). In addition, IHC analysis of the phosphorylated form of AXL (pAXL) and PDGFRα with 66 GBM patients exhibited the same pattern of expression (Fig. 1D and E). When we investigated the intra-tumoral spatial difference of AXL and PDFGRα using the IVY GBM Atlas Project database, AXL was expressed at significantly higher levels in areas of vascular proliferation, whereas cellular tumor areas

had significantly higher expression of PDGFRα compared to other areas (Fig. 1F). These data indicate the inter-tumoral and intra-tumoral inverse correlation of AXL activation and PDGFRα expression in GBM tumors and GSCs.

Next, we investigated whether the inverse expression of AXL and PDGFRα is due to a secondary enrichment of AXL(+) cells in MES GBMs or to a loss of PDGFRα, which in turn directly causes AXL upregulation. We therefore conducted *in situ* hybridization experiments using molecular beacon (MB) probes. We performed live monitoring of PDGFRα (FAM-labeled: green) and AXL (CY5-labeled: violet) at the single cell level (Fig. 1G and Supplementary Fig. S1B). The induction of AXL upregulation was directly captured by clonal tracking of GSC157 transfected with siRNA for PDGFRα, indicating that the reduction of PDGFRα leads to upregulation of AXL in a single cell.

Previously, we and others reported an association between MES GSC signature and increased glycolytic activity (19). Therefore, we compared lactic acid levels and the extracellular acidification rate (ECAR) in GSCs expressing non-targeting shRNA or shRNA targeting AXL to determine whether AXL knockdown alters GSC glycolytic activity. AXL knockdown in two patient-derived GSCs (GSC83 and GSC326) was associated with a decrease in lactic acid levels and ECAR. In addition, ECAR-associated compensation, reflective of a shift toward glycolysis due to a shut-off of mitochondrial reserve capacity, was attenuated by AXL knockdown in these samples (Fig. 1H and I). Analysis of microarray data also indicated that AXL is associated with a set of genes involved in the glycolysis pathway (Fig. 1J). Thus, these data indicate that reduced expression of AXL *in vitro* results in a concomitant decrease in glycolytic activity.

BGB324 inhibits survival and growth more effectively in GSC-derived GBM tumors expressing higher levels of AXL *in vivo*

Next, we tested the effects of the small molecule AXL inhibitor BGB324 on GSCs *in vitro* and on GSC-derived mouse tumors *in vivo* (Fig. 2). We used five patient-derived GSCs; three cell lines expressed higher levels of AXL (AXL high), while two expressed lower levels (AXL low). We found that the *in vitro* efficacy of BGB324 is related to AXL expression levels: GSC growth is more inhibited in lines with higher AXL levels than in lines with lower levels of the protein (Fig. 2A). Using Western blot analysis, we confirmed that AXL phosphorylation, an indicator of activity, is decreased in GSC267 cells (AXL high) after treatment with BGB324 (Fig. 2B).

We then tested the ability of BGB324 to promote survival of mice injected with cells from two GSC-derived mouse tumors. BGB324 treatment provided a marked survival benefit for mice bearing GSC267 (AXL high)-derived intracranial tumors and, to a lesser extent, for those bearing the GSC374 (AXL low)-derived tumors (Fig. 2C). Two days after completion of BGB324 treatment, we performed IHC on tumor samples derived from GSC267 treated mice. We found that pAXL is largely absent in tumors treated with BGB324, but is abundantly expressed in the control tumors (Fig. 2D). In contrast, the population of tumor cells positive for Caspase-3 and pH2A.X, proteins expressed during apoptosis, was markedly increased in BGB324-treated tumors. These results indicate that BGB324-mediated

inactivation of AXL in GSCs promotes apoptosis in tumor cells, leading to reduced tumor-burdens in mice a survival benefit.

Tumor-associated microglia/macrophages (MG/Mø) activate AXL in GSCs

Recent studies, including ours, have found that MES GBM tumors tend to have more immune reactive modulation compared to the other subtypes (26–29). In addition, one study reported that tumor-associated MG/ Mø comprised 30% to 50% of the tumor mass in GBM (30). Infiltrating Mø constituted approximately 85% of the total tumor-associated MG/Mø, while resident MG comprised approximately 15% of the MG/Mø (31). We performed IHC analysis of MES GBM patient tissues (Fig. 3A) and tissues from the two GSC-derived mouse tumor models (Fig. 3B) to detect expression of CD11b, a marker for tumor-associated MG/Mø. We found that CD11b(+) MG/Mø are highly enriched in perivascular area of MES GBM tissues. In addition, there was a marked increase in the number of CD11b(+) cells in GSC267 (AXL high)-derived tumor samples as compared to GSC374 (AXL low)-derived tumor samples from the xenograft model (Fig. 3B). We then sought to determine whether CD11b(+) cells affect tumor growth. To this end, we used a mouse GSC line derived from genetically-engineered mice with deletions of Pten, p53, and Nf1 (20). We treated mice bearing the mouse GSC-derived tumors with the CSF-1R inhibitor, BLZ945 in order to prevent the recruitment of CD11b(+) cells. The prevention of their recruitment was first confirmed by IHC (Supplemental Fig. S2A and B). H&E staining of the treated mouse brains showed that the tumor volumes of the BLZ945-treated group are significantly smaller than the control group (Fig. 3C), suggesting that CD11b(+) cells promote GBM growth in mouse brains. Next, we asked if AXL expression in MES GSCs is affected by CD11b(+) cells. To address this question, we first isolated and cultured CD11b(+) cells from GSC267-derived mouse tumors (Fig. 3D). We then treated GSC267 cells with conditioned media from the purified CD11b(+) cells and measured the levels of total- and pAXL. We found that the expression of pAXL, but not total AXL, is markedly increased by treatment with this conditioned media (Fig. 3E). In turn, we sought to test whether AXL contributes to recruitment of CD11b(+) cells into GBM tumors. To address this question, we performed shRNA-mediated AXL knockdown in mouse GBM tumors. As shown in Fig. 3F, decreased infiltration of CD11b(+) cells in mouse GBM tumors was observed by AXL knockdown. Collectively, these data suggest that AXL in MES GSCs and CD11b(+) cells have crosstalk to promote tumor growth in mouse brains.

MG/Mø-derived PROS1 binds and activates AXL in GSCs

TAM family receptors have two known ligands, GAS6 and PROS1; data suggest that GAS6 is the only ligand responsible for AXL activation (2). To identify the regulatory ligand(s) required for AXL activation in GSCs, we analyzed the IVY GBM Atlas dataset. Unlike the other two TAM receptors, AXL was highly expressed in the areas of vascular proliferation within GBM tumors (Fig. 4A). In contrast, GAS6 exhibited a different localization pattern. Among the four intra-tumoral regions, its expression was lowest in the vascular proliferation area. Unexpectedly, PROS1 showed relatively higher expression in the vascular proliferation area.

Using an ELISA assay, we detected PROS1 in conditioned media from CD11b(+) cells isolated from GSC267-derived mouse tumors (Fig. 4B); this finding suggests that MG/Mø associated with MES tumors secrete PROS1 protein. When GSC267 cells were treated with recombinant PROS1 protein, we observed a marked increase of pAXL, but not total-AXL protein levels (Fig. 4C). We then measured AXL activation levels in GSC267 cells in the presence of a PROS1 blocking peptide together with the conditioned medium from CD11b(+) MG/Mø isolated from the GSC-bearing mice. As shown in Fig. 4D, the phosphorylation of AXL is dramatically decreased by PROS1 blocking peptide. These data suggest that tumor-associated MG/Mø activate AXL signaling in GSCs via a PROS1-dependent pathway.

The above results led us to ask whether PROS1 physically associates with AXL. We incubated cell lysates from two patient-derived MES GSCs (GSC267 and GSC1020) with Histidine (His)-tagged PROS1 and performed immunoprecipitation assays, followed by Western blot analysis. Using antibodies to AXL, His-tagged PROS1 was co-immunoprecipitated with AXL; similarly, AXL was co-immunoprecipitated with PROS1 using Ni-NTA beads (Fig. 4E and Supplementary Fig. S3A–C). In both GSC lines, the data obtained from IP assays and Western blot analysis revealed an interaction between PROS1 and AXL.

We next investigated the effect of PROS1 on cell growth of three GSC lines (GSC267, 28, and 1020). PROS1 promoted sphere growth in serum-free media; this growth was strongly suppressed by addition of BGB324 in a dose-dependent manner (Fig. 4F). We then investigated the downstream targets of PROS1-mediated signaling in GSCs. Our previous studies identified NF-κB activation in MES GBM (32), therefore, we specifically looked into this pathway in GSCs. Treatment of GSC267 cells with PROS1 increased levels of both phosphorylated AXL and p65, a subunit of the NF-κB complex, without noticeable changes in the total levels of either protein (Fig. 4G). This PROS1-mediated p65 activation was eliminated by treatment with BGB324 (Fig. 4H and Supplementary Fig. S3D–G). Consistent with these results, GSEA exhibited that genes affected by AXL silencing in GSC cells are associated with the NF-κB pathway signature (Fig. 4I). Taken together, these data indicated that PROS1 secreted by MG/Mø interacts with AXL in MES GSCs, leading to its phosphorylation, thereby regulating the NF-κB signaling to promote GBM tumor growth.

Combined treatment of mouse GBM with BGB324 and PD-1 inhibitor Nivolumab enhances survival

A recent study has indicated that increased rates of glycolysis in cancer cells suppress T cell function (33). As our data in Fig. 1H and I showed that AXL expression is positively correlated with glycolysis, we speculated that increase of AXL expression might suppress immune function in the tumor microenvironment. To analyze the population of immune cells in GBM, we first used metal-labeled probes and mass spectrometric analysis (cytometry by time-of-flight, or CyTOF) of freshly-dissociated GBM patient tissues (424; newly-diagnosed and 378; recurrent tumors). These single-cell dissociates were labeled with CD45, CD3, CD4, CD8, and PD-1 antibodies conjugated with different heavy metals. These markers allowed us to determine the presence of various immune cell populations and their

expression of this B7 family member in individual cells. Following this labeling procedure, we performed t-Distribution Stochastic Embedding (t-SNE) analysis to detect the CD4+ and CD8+ T cells within these tumors. We then specifically analyzed expression of PD-1 protein on these T cell populations. The results showed PD-1 is expressed in both CD4 (16.9%) and CD8 T (48.6%) cells as compared to negative control of primary GBM dissociated cells (Fig. 5A and B and Supplementary Fig. S4). In addition, we analyzed the population of immune cells in our syngeneic mouse model using flow cytometry. The results showed that high frequencies of GBM-infiltrating, activated T cells (CD4 and CD8; 50~80%) express PD-1. BGB324 treatment had no effect on either percentage of activated CD4 or CD8 T cells expressing PD-1 or on the intensity of PD-1 expression on these cell populations (Fig. 5C and D). On the other hand, the transcriptomic analysis of the BGB324 treated mouse GBM tumors showed mixed results of the expression of the B7 family (Fig. 5E). In particular, PD-L1 was downregulated, while PD-L2 was upregulated by BGB324 treatment. We also confirmed this regulation *in vitro* experiment (Supplementary Fig. S5A–E). ICOSLG, VISTA, and CD276 were also upregulated, which are other immune checkpoint regulators in various cancers. Flow cytometry analysis of mouse tumors showed that the majority of PD-L1 or PD-L2 expressing cells in the tumor environment are CD45(−) cells, which consists primarily of tumor cells. A modest percentage of CD45(+)/CD11b(+) cells (MG/Mø) also express PD-L1. However, CD45(+)/CD11b(+) cells (MG/Mø) express higher level of PD-L1 and PD-L2 on a per cell basis then other leukocyte (CD45(+)/CD11b(−)) or non-immune (CD45(−)) populations (Supplementary Fig. S5F and G). Collectively, the high expression of PD-1 and its ligands on multiple cell types within GBM tumors suggest that a therapy based upon PD-1 blockade could be effective in GBM.

As of January 2018, four clinical trials with the PD-1 inhibitor Nivolumab have been designed for GBM. In contrast to the encouraging results obtained for some cancers such as melanoma, the first one for GBM, which was designed to compare the efficacy of Nivolumab vs. Bevacizumab on recurrent tumors, was completed recently and turned out negative (34). Given that some recent papers indicate that AXL is associated with immune suppression (35,36), we hypothesized that the combined treatment of Nivolumab with BGB324 may provide additive, or possibly synergistic, anti-tumor effects. To investigate the AXL/PD-L1 signaling axis in an immune-competent model, we used mouse GSCs (MS6989 and MS7080) harvested from spontaneously-formed GBM-like tumors isolated from mice. These syngeneic mouse GBM models were then treated with BGB324; we found that the IC_{50} for BGB324 in MS6989 and MS7080 sphere cultures *in vitro* was 0.768 μM and 0.9521 μM, respectively, values comparable with those for human GSCs (Supplementary Fig. S6A). Using these mouse GBM models, we investigated the changes of MG/Mø expression and their downstream effector proteins in Nivolumab-treated mouse GBMs. As shown in Figure 5F, PD-1 blocking Ab treatment increased the proportion of CD11b-expressing MG/Mø in these mouse tumors. Furthermore, pAXL expression was substantially elevated in these tumors (Fig. 5G). Interestingly, BGB324 treatment significantly reduced the frequencies of infiltrating CD45(+) leukocytes and CD11b(+) MG/Mø cells, whereas the treatment had no effect on the frequencies of CD4 or CD8 T cells (Fig. 5H). In addition, PD-1 antibody treatment has no effect on the frequency of total or activated (CD44(+)) tumor-infiltrating CD4(+) or CD8(+) T cells that express PD-1 (Supplementary Fig. S6B

and C). We then examined the efficacy of these therapeutic agents on mouse GBMs. Treatment with Nivolumab alone for MS7080 xenograft mice did not enhance survival *in vivo* (Fig. 5I and Supplementary Fig. S6D), consistent with the recent data from the clinical trial for human GBMs. In contrast, in mice with MS6989 or MS7080-derived tumors, combined treatment with BGB324 and the PD-1 antibody resulted in an increased survival (Fig. 5J and Supplementary Fig. S6E). Together, these data suggest that combined treatment with BGB324 and Nivolumab may provide a potential therapeutic approach for GBM treatment.

Expression of AXL and/or PROS1 is associated with a poor prognosis for GBM patients

Lastly, we investigated the clinical relevance of our pre-clinical findings by using The Cancer Genome Atlas (TCGA) database. The log-rank test showed that glioma patients with higher AXL protein expression had poorer survival compared with patients whose tumors had lower AXL protein expression levels (Fig. 6A), while survival of patients with higher PROS1-expressed tumors did not show a significant difference from those with low PROS1-expressed tumors. Interestingly, glioma patients with lower AXL and PROS1 expression had better survival compared with the other patient groups. Collectively, these results indicate that PROS1 activates AXL in MES GSCs and is negatively linked to post-surgical survival of patients with GBM tumors.

Discussion

In this study, we uncovered novel mechanisms associated with AXL signaling in GBM and GSCs. First, we identified a negative correlation between the expression of PDGFRα and pAXL in GSCs and in GBM tumors. We then showed that treatment of MES GSC-derived mouse tumors with BGB324, an inhibitor of AXL, decreased tumor growth, thereby providing a survival benefit. We also observed that treatment with conditioned media derived from tumor-associated MG/Mø cells promotes AXL signaling in GSCs and that PROS1 secreted from MG/Mø cells binds to, and activates AXL in GSCs, leading to increased GSC growth. Consistent with an *in vivo* role for this signaling pathway, combined treatment with BGB324 and PD-1 blocking antibody effectively prolonged the survival of immunocompetent mice bearing syngeneic GBM tumors. Finally, we report high AXL and/or PROS1 expression is associated with a poor prognosis in GBM patients.

Our study is the first to demonstrate a role for PROS1-mediated AXL signaling in cancer, which is negatively regulated by PDGFRα. To our knowledge, GAS6 is the only previously known ligand for AXL (37–40). However, a recent study reported that in oral squamous carcinoma cells, PROS1 plays a role in promoting tumor growth and may act as a modulator of AXL expression (41). In our study, we unexpectedly observed that PROS1 is secreted from CD11b(+) MG/Mø cells, which are highly enriched in the perivascular area of MES GBM tissues; upon secretion, PROS1 binds to, and subsequently activates AXL in GSCs. We also observed that the NFκB pathway is upregulated upon AXL activation in GSCs (Fig. 6B). However, it remains to be determined whether the NFκB pathway is the major downstream target of the PROS1-AXL signaling axis in GSCs.

The AXL inhibitor BGB324 is currently under evaluation in two Phase I/II clinical trials, including in AML; BGB324 has produced promising initial results for its tolerability and anti-leukemic activity (42). Using the conventional GBM cell lines, an experimental study has shown that BGB324 inhibits *in vitro* growth, migration, and invasion (43). To extend these observations, we used our well-characterized patient-derived pre-clinical GSC models to determine the effects of BGB324 on both *in vitro* clonogenicity and *in vivo* tumor initiation and propagation. Our data show that BGB324 substantially promotes survival of immunocompromised mice harboring human GSC-derived mouse xenograft tumors. In GBM tumors from mice treated with BGB324, we found increased expression of B7 family members, including ICOSLG, VISTA, and CD276. Interestingly, treatment with an anti-VISTA antibody was previously shown to increase immune cell infiltration in prostate cancer (44). Therefore, upregulation of some B7 family members may be another pro-tumorigenic pathway activated in GBM. Further studies are needed to address this question.

We also found that after treatment with PD-1 blocking antibody, there was no significant difference in the survival of mice bearing mouse GSC-derived tumors compared to the untreated control group. Similarly, responses to single-agent immune checkpoint inhibitors, such as CTLA-4- and PD-1/PD-L1-targeted mAbs, have been limited to 10% to 30% (45). Furthermore, results from the first clinical trial with the PD-1 antibody for the treatment of recurrent GBM were negative (34). Given that an immune checkpoint inhibitor alone may not be sufficient for treatment of GBM, new combination treatments are likely needed. In a recent study, AXL was found to be a key gene expressed in metastatic melanoma patients that were unresponsive to PD-1 immunotherapy (36). Consistent with a role for AXL in modulating immunotherapeutic efficacy, here we found that combination treatment with BGB324 and anti-PD-1 effectively prolonged the survival of immunocompetent mice bearing syngeneic GBM tumors. Currently, we are developing a clinical trial for the treatment of recurrent GBM using BGB324 monotherapy with an intention to subsequently extend to a BGB324/Nivolumab combination.

Our findings reveal several intriguing questions that will guide future investigations. First, the mice treated with PD-1 antibody showed an increase of CD11b(+) tumor-associated MG/Mø cells and increased expression of pAXL and PROS1. These findings suggest that PD-1 antibody treatment recruits more CD11b(+) MG/Mø cells to GBM tumors, resulting in an increase of pAXL and PROS1 expression. A possible explanation for our observations is that PD-1-targeted antibody binds to PD-1 on MG/Mø cells associated with GBM tumors, thereby causing the infiltrated MG/Mø cells to express factors that subsequently recruit more MG/Mø cells. Next, our data illustrate that BGB324 promoted apoptosis of tumor cells, decreased intratumoral CD11b(+) cells, and blocked AXL phosphorylation in GSC xenografts. Collectively, these findings suggest that the enhanced efficacy of combined anti-PD-1 and BGB324, relative to either anti-PD-1 or BGB324 alone, is due to multiple complementary effects of these agents. First, BGB324 is likely counteracting the increased infiltration of PROS1-secreting CD11b(+) cells that occurs in response to anti-PD-1. Second, BGB324 is preventing AXL signaling from promoting GBM progression. Lastly, anti-PD-1 is likely increasing the duration and magnitude of the anti-tumor T cell response, as has been seen in other models. Collectively, these differential effects on tumor cells and

immune cells result in enhanced efficacy of the combination treatment, as seen by prolonged survival. Further experiments are needed to clarify these assumptions.

Of note, we found that BGB324 efficacy is significantly different between human cell xenograft models in immunocompromised mice and the syngeneic mouse tumor models in immunocompetent mice, though the IC_{50} ranges of BGB324 in human and mouse GBM cells are comparable. As stated above, we speculate that the immune microenvironment plays a key role in the BGB324 sensitivity of GBM tumors. Given that human GBM arises under an immune-suppressed condition with extensive steroid treatment, it is tempting to predict that results from the first surgical pharmacokinetics clinical trial study using BGB324 for the treatment of human recurrent GBM will show some efficacy.

In conclusion, this study identified that tumor-associated MG/Mø cells produce PROS1 that binds and activates AXL in GSCs. The PROS1/AXL signaling axis in GSCs subsequently activates the tumor-intrinsic NFκB pathway to promote the MES phenotype of GBM tumors. In addition, we found that combination treatment with BGB324 and the PD-1 antibody effectively increases the survival of immunocompetent mice bearing syngeneic GBM tumors. Taken together, our data suggest that the combination treatment of AXL and immune checkpoint inhibitors may be a promising new therapeutic approach for the treatment of GBM.

Supplementary Material

Refer to Web version on PubMed Central for supplementary material.

Acknowledgments

We thank all the members of the Nakano laboratory for constructive discussion of this study. This study was supported by following NIH grants: P01CA163205 (I. Nakano); R01NS083767 (I. Nakano); R21CA175875 (I. Nakano); R01NS087913 (I. Nakano); R01CA183991 (I. Nakano).

References

1. Cheng P, Phillips E, Kim SH, Taylor D, Hielscher T, Puccio L, et al. Kinome-wide shRNA screen identifies the receptor tyrosine kinase AXL as a key regulator for mesenchymal glioblastoma stem-like cells. Stem Cell Reports. 2015; 4:899–913. [PubMed: 25921812]
2. Graham DK, DeRyckere D, Davies KD, Earp HS. The TAM family: phosphatidylserine sensing receptor tyrosine kinases gone awry in cancer. Nature reviews Cancer. 2014; 14:769–85. [PubMed: 25568918]
3. Stitt TN, Conn G, Gore M, Lai C, Bruno J, Radziejewski C, et al. The anticoagulation factor protein S and its relative, Gas6, are ligands for the Tyro 3/Axl family of receptor tyrosine kinases. Cell. 1995; 80:661–70. [PubMed: 7867073]
4. Varnum BC, Young C, Elliott G, Garcia A, Bartley TD, Fridell Y-W, et al. Axl receptor tyrosine kinase stimulated by the vitamin K-dependent protein encoded by growth-arrest-specific gene 6. Nature. 1995; 373:623–6. [PubMed: 7854420]
5. Ben-Batalla I, Schultze A, Wroblewski M, Erdmann R, Heuser M, Waizenegger JS, et al. Axl, a prognostic and therapeutic target in acute myeloid leukemia mediates paracrine crosstalk of leukemia cells with bone marrow stroma. Blood. 2013; 122:2443–52. [PubMed: 23982172]
6. Asiedu MK, Beauchamp-Perez FD, Ingle JN, Behrens MD, Radisky DC, Knutson KL. AXL induces epithelial-to-mesenchymal transition and regulates the function of breast cancer stem cells. Oncogene. 2013; 33:1316–24. [PubMed: 23474758]

7. Sheridan C. First Axl inhibitor enters clinical trials. Nature biotechnology. 2013; 31:775–6.
8. Skinner HD, Giri U, Yang LP, Kumar M, Liu Y, Story MD, et al. Integrative Analysis Identifies a Novel AXL-PI3 Kinase-PD-L1 Signaling Axis Associated with Radiation Resistance in Head and Neck Cancer. Clin Cancer Res. 2017; 23:2713–22. [PubMed: 28476872]
9. Wolchok JD. PD-1 Blockers. Cell. 2015; 162:937. [PubMed: 26317459]
10. Larkin J, Chiarion-Sileni V, Gonzalez R, Grob J, Cowey LC, Lao CD, et al. Combined Nivolumab and Ipilimumab or Monotherapy in Untreated Melanoma. The New England Journal of Medicine. 2015; 373:23–34. [PubMed: 26027431]
11. Fecci PE, Ochiai H, Mitchell DA, Grossi PM, Sweeney AE, Archer GE, et al. Systemic CTLA-4 Blockade Ameliorates Glioma-Induced Changes to the CD4+ T Cell Compartment without Affecting Regulatory T-Cell Function. Clinical Cancer Research. 2007; 13:2158–67. [PubMed: 17404100]
12. Reardon DA, Gokhale PC, Klein SR, Ligon KL, Rodig SJ, Ramkissoon SH, et al. Glioblastoma Eradication Following Immune Checkpoint Blockade in an Orthotopic, Immunocompetent Model. Cancer Immunology Research. 2016; 4:124–35. [PubMed: 26546453]
13. Zeng J, See AP, Phallen J, Jackson CM, Belcaid Z, Ruzevick J, et al. Anti-PD-1 Blockade and Stereotactic Radiation Produce Long-Term Survival in Mice With Intracranial Gliomas. International Journal of Radiation Oncology*Biology*Physics. 2013; 86:343–9.
14. Huang J, Liu F, Liu Z, Tang H, Wu H, Gong Q, et al. Immune Checkpoint in Glioblastoma: Promising and Challenging. Frontiers in Pharmacology. 2017; 8:242. [PubMed: 28536525]
15. Kamran N, Calinescu A, Candolfi M, Chandran M, Mineharu Y, Asad AS, et al. Recent advances and future of immunotherapy for glioblastoma. Expert Opinion on Biological Therapy. 2016; 16:1–20.
16. Preusser M, Lim M, Hafler DA, Reardon DA, Sampson JH. Prospects of immune checkpoint modulators in the treatment of glioblastoma. Nature Reviews Neurology. 2015; 11:504–14. [PubMed: 26260659]
17. Kim E, Kim M, Woo DH, Shin Y, Shin J, Chang N, et al. Phosphorylation of EZH2 activates STAT3 signaling via STAT3 methylation and promotes tumorigenicity of glioblastoma stem-like cells. Cancer Cell. 2013; 23:839–52. [PubMed: 23684459]
18. Kim SH, Joshi K, Ezhilarasan R, Myers TR, Siu J, Gu C, et al. EZH2 protects glioma stem cells from radiation-induced cell death in a MELK/FOXM1-dependent manner. Stem Cell Reports. 2015; 4:226–38. [PubMed: 25601206]
19. Mao P, Joshi K, Li J, Kim S-HH, Li P, Santana-Santos L, et al. Mesenchymal glioma stem cells are maintained by activated glycolytic metabolism involving aldehyde dehydrogenase 1A3. Proceedings of the National Academy of Sciences of the United States of America. 2013; 110:8644–9. [PubMed: 23650391]
20. Alcantara Llaguno S, Chen J, Kwon C-H, Jackson EL, Li Y, Burns DK, et al. Malignant Astrocytomas Originate from Neural Stem/Progenitor Cells in a Somatic Tumor Suppressor Mouse Model. Cancer Cell. 2009; 15:45–56. [PubMed: 19111880]
21. Chang L, Gallego-Perez D, Zhao X, Bertani P, Yang Z, Chiang CL, et al. Dielectrophoresis-assisted 3D nanoelectroporation for non-viral cell transfection in adoptive immunotherapy. Lab Chip. 2015; 15:3147–53. [PubMed: 26105628]
22. Gallego-Perez D, Chang L, Shi J, Ma J, Kim SH, Zhao X, et al. On-Chip Clonal Analysis of Glioma-Stem-Cell Motility and Therapy Resistance. Nano Lett. 2016; 16:5326–32. [PubMed: 27420544]
23. Simoni Y, Fehlings M, Kløverpris HN, McGovern N, Koo S-L, Loh C, et al. Human Innate Lymphoid Cell Subsets Possess Tissue-Type Based Heterogeneity in Phenotype and Frequency. Immunity. 2017; 46:148–61. [PubMed: 27986455]
24. Finck R, Simonds EF, Jager A, Krishnaswamy S, Sachs K, Fantl W, et al. Normalization of mass cytometry data with bead standards. Cytometry Part A. 2013; 83A:483–94.
25. Cheng P, Wang J, Waghmare I, Sartini S, Coviello V, Zhang Z, et al. FOXD1-ALDH1A3 Signaling Is a Determinant for the Self-Renewal and Tumorigenicity of Mesenchymal Glioma Stem Cells. Cancer research. 2016; 76:7219–30. [PubMed: 27569208]

26. Beier CP, Kumar P, Meyer K, Leukel P, Bruttel V, Aschenbrenner I, et al. The Cancer Stem Cell Subtype Determines Immune Infiltration of Glioblastoma. Stem Cells and Development. 2012; 21:2753–61. [PubMed: 22676416]
27. Bhat KPLPL, Balasubramaniyan V, Vaillant B, Ezhilarasan R, Hummelink K, Hollingsworth F, et al. Mesenchymal differentiation mediated by NF-κB promotes radiation resistance in glioblastoma. Cancer cell. 2013; 24:331–46. [PubMed: 23993863]
28. Doucette T, Rao G, Rao A, Shen L, Aldape K, Wei J, et al. Immune Heterogeneity of Glioblastoma Subtypes: Extrapolation from the Cancer Genome Atlas. Cancer Immunology Research. 2013; 1:112–22. [PubMed: 24409449]
29. Rutledge CW, Kong J, Gao J, Gutman DA, Cooper L, Appin C, et al. Tumor-Infiltrating Lymphocytes in Glioblastoma Are Associated with Specific Genomic Alterations and Related to Transcriptional Class. American Association for Cancer Research. 2013; 19:4951–60.
30. Charles NA, Holland EC, Gilbertson R, Glass R, Kettenmann H. The brain tumor microenvironment. Glia. 2012; 60:502–14. [PubMed: 22379614]
31. Chen Z, Feng X, Herting CJ, Garcia VA, Nie K, Pong WW, et al. Cellular and Molecular Identity of Tumor-Associated Macrophages in Glioblastoma. Cancer research. 2017; 77:2266–78. [PubMed: 28235764]
32. Kim S-HH, Ezhilarasan R, Phillips E, Gallego-Perez D, Sparks A, Taylor D, et al. Serine/Threonine Kinase MLK4 Determines Mesenchymal Identity in Glioma Stem Cells in an NF-κB-dependent Manner. Cancer cell. 2016; 29:201–13. [PubMed: 26859459]
33. Ho PC, Bihuniak JD, Macintyre AN, Staron M, Liu X, Amezquita R, et al. Phosphoenolpyruvate Is a Metabolic Checkpoint of Anti-tumor T Cell Responses. Cell. 2015; 162:1217–28. [PubMed: 26321681]
34. Reardon DA, Omuro A, Brandes AA, Rieger J, Wick A, Sepulveda J, et al. OS10.3 Randomized Phase 3 Study Evaluating the Efficacy and Safety of Nivolumab vs Bevacizumab in Patients With Recurrent Glioblastoma: CheckMate 143. Neuro-Oncology. 2017; 19
35. Aguilera TA, Rafat M, Castellini L, Shehade H, Kariolis MS, Hui AB, et al. Reprogramming the immunological microenvironment through radiation and targeting Axl. Nat Commun. 2016; 7:13898. [PubMed: 28008921]
36. Hugo W, Zaretsky JM, Sun L, Song C, Moreno B, Hu-Lieskovan S, et al. Genomic and Transcriptomic Features of Response to Anti-PD-1 Therapy in Metastatic Melanoma. Cell. 2016; 165:35–44. [PubMed: 26997480]
37. Antony J, Tan T, Kelly Z, Low J, Choolani M, Recchi C, et al. The GAS6-AXL signaling network is a mesenchymal (Mes) molecular subtype–specific therapeutic target for ovarian cancer. Sci Signal. 2016; 9
38. Hutterer M, Knyazev P, Abate A, Reschke M, Maier H, Stefanova N, et al. Axl and Growth Arrest–Specific Gene 6 Are Frequently Overexpressed in Human Gliomas and Predict Poor Prognosis in Patients with Glioblastoma Multiforme. Clinical Cancer Research. 2008; 14:130–8. [PubMed: 18172262]
39. Rankin EB, Fuh KC, Castellini L, Viswanathan K, Finger EC, Diep AN, et al. Direct regulation of GAS6/AXL signaling by HIF promotes renal metastasis through SRC and MET. Proceedings of the National Academy of Sciences. 2014; 111:13373–8.
40. Shiozawa Y, Pedersen EA, Patel LR, Ziegler AM. GAS6/AXL axis regulates prostate cancer invasion, proliferation, and survival in the bone marrow niche. GAS6/AXL axis regulates prostate cancer invasion, proliferation, and survival in the bone marrow niche. 2010
41. Abboud-Jarrous G, Priya S, Maimon A, Fischman S, Cohen-Elisha M, Czerninski R, et al. Protein S drives oral squamous cell carcinoma tumorigenicity through regulation of AXL. Oncotarget. 2014; 5
42. Loges S, Gjertsen B, Heuser M, Ben-Batalla I, Micklem D, Jorg C, et al. A first-in-patient phase I study of BGB324, a selective Axl kinase inhibitor in patients with refractory/relapsed AML and high-risk MDS. American Society of Clinical Oncology. 2016
43. Vouri M, An Q, Birt M, Pilkington GJ, Hafizi S. Small molecule inhibition of Axl receptor tyrosine kinase potently suppresses multiple malignant properties of glioma cells. Oncotarget. 2015; 6:16183–97. [PubMed: 25980499]

44. Gao J, Ward JF, Pettaway CA, Shi LZ, Subudhi SK, Vence LM, et al. VISTA is an inhibitory immune checkpoint that is increased after ipilimumab therapy in patients with prostate cancer. Nature Medicine. 2017; 23:551–5.

45. Aguilera TA, Giaccia AJ. Molecular Pathways: Oncologic Pathways and Their Role in T-cell Exclusion and Immune Evasion—A New Role for the AXL Receptor Tyrosine Kinase. Clinical Cancer Research. 2017; 23:2928–33. [PubMed: 28289089]

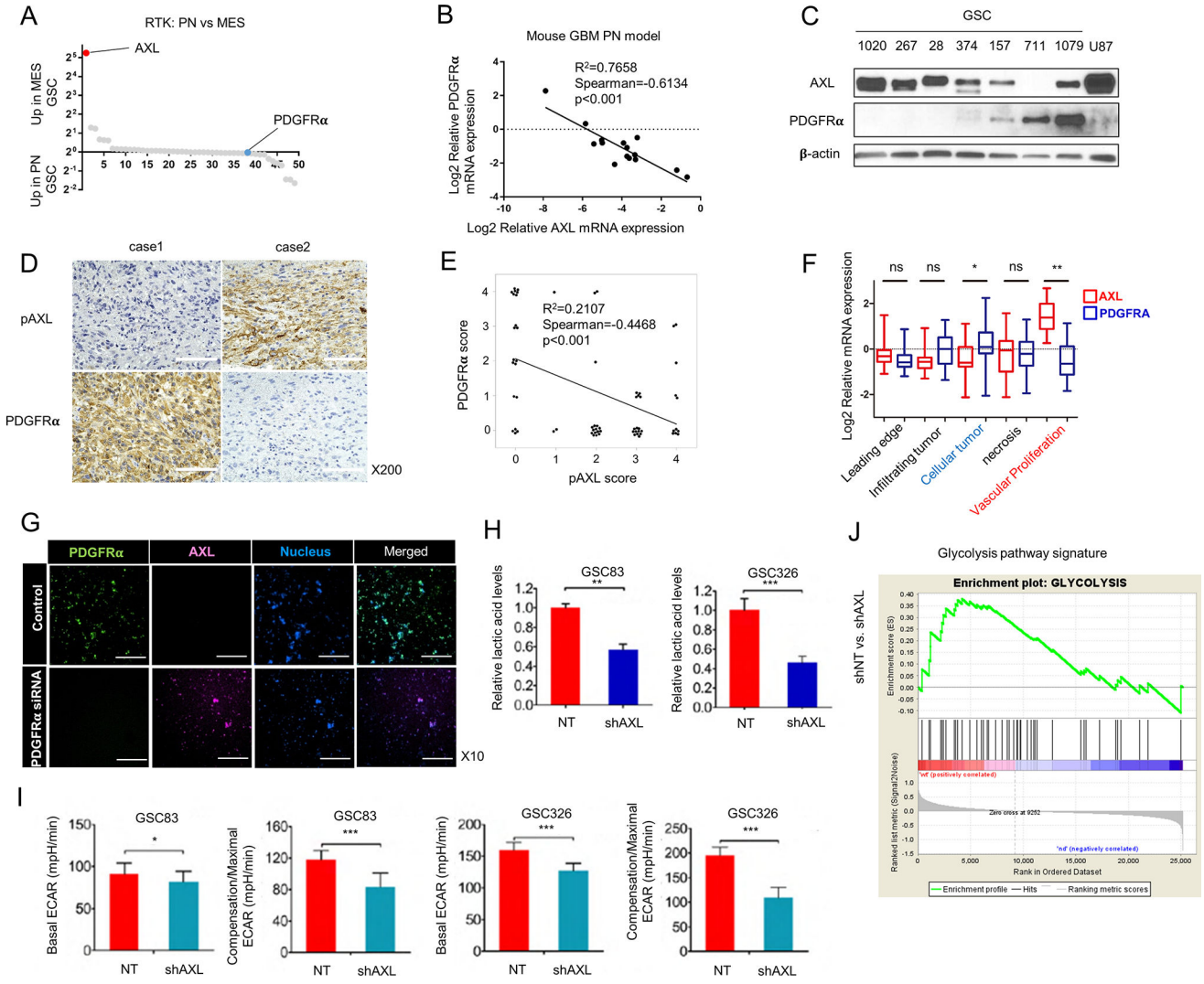

Figure 1.

Expression of AXL is negatively correlated with PDGFRα expression in glioma sphere models. **A.** Transcriptome microarray analysis (GSE67089) of the relative mRNA expression levels of 49 RTKs in samples from 15 MES and 12 PN GSCs. AXL is the most highly expressed RTK in MES GSCs, while PDGFRα is expressed at the lowest level in GSCs. **B.** qRT-PCR analysis of AXL and PDGFRα expression levels in samples from a PDGFB overexpression mouse glioma model. The mRNA expression pattern of the two genes has a negative correlation (n = 15, $R^2 = 0.7658$, Spearman = −0.6134, $P < 0.001$). **C.** A representative Western blot showing the negative correlation between PDGFRα and AXL protein expression in samples from 7 GSCs and the U87 cell line; β-Actin served as a loading control. **D** and **E**. Expression of PDGFRα and phospho-AXL in human GBM tissues is mutually exclusive. Expression of PDGFRα and pAXL was analyzed in tumor samples from 66 patients (37 males; 29 females; median age, 56) with GBM. Fresh tumor tissues were obtained by biopsy or surgery from 1998 to 2016 at Kanazawa University. Representative IHC images are shown (**D**). Case 1 GBM shows positive cytoplasmic expression of PDGFRα and negative pAXL expression. Case 2 GBM shows negative

PDGFRα expression, but a positive expression of pAXL at the membranes. Scale bars, 100 μm. (**E**). Analysis of PDGFRα and pAXL expression in 66 samples show that expression is mutually exclusive (n = 66, R^2 = 0.2107, Spearman = −0.4468, $P < 0.001$). **F.** Data from the IVY Atlas Project Database revealed that AXL and PDGFRα are enriched in different tumor regions (**$P < 0.001$, ***$P < 0.0001$, t-test). **G**. Fluorescent images of control group and PDGFRα siRNA group with PDGFRα (green: FAM) and AXL (red: CY5) molecular beacons. Scale bars, 250 μm. **H.** Graphical representation of the relative lactic acid levels in MES cell lines expressing non-targeting shRNAs (NT) and shRNAs targeting AXL (shAXL). Two different MES cell lines, GSC83 and GSC326, were tested (**$P < 0.05$, *** $P < 0.001$). **I.** Graphical representation of the basal extracellular acidification rate (ECAR) and compensation/maximal ECAR in MES cell lines expressing NT and shAXL (*$P < 0.05$, *** $P < 0.0001$). **J**. GSEA showing glycolysis (right) signature is reduced in AXL-depleted GSCs. The normalized enrichment score (NES) is shown in the plot.

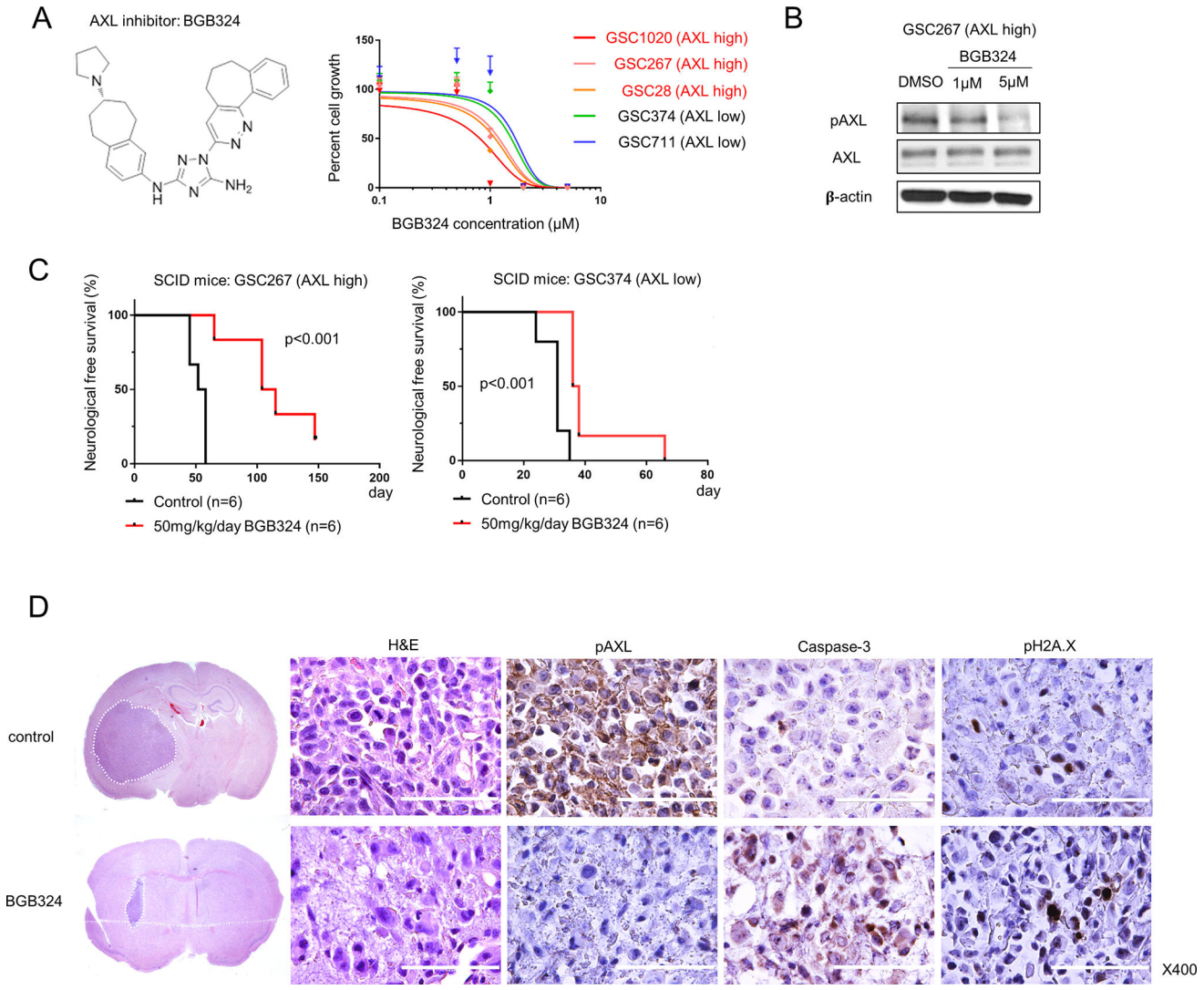

Figure 2.

BGB324 treatment inhibits AXL activity more effectively in cells with high levels of AXL expression. **A.** The molecular structure of BGB324, an AXL inhibitor (left) and a graphical representation showing that BGB324 inhibition of AXL in several GSCs results in a decrease in cell growth (right). The IC_{50} for BGB324 in cells expressing high levels of AXL is lower than that in cells expressing low levels of AXL. **B.** Western blot analysis shows that after 3 days of treatment with 1 or 5 μM BGB324, AXL is dephosphorylated in GSC267 cells. **C.** Kaplan-Meier survival curves generated from data obtained from xenograft mice inoculated with either GSC267 (AXL high) or GSC374 (AXL low) cells, with and without BGB324 treatment for 10 days (log-rank test). **D.** Representative hematoxylin and eosin (H&E) staining and IHC of GSC267 xenografts after 10 days of BGB324 treatment. In the H&E-stained coronal sections, white broken lines show the tumor area. Positive staining for Caspase 3 and pH2A.X indicates apoptosis. Scale bars, 100 μm.

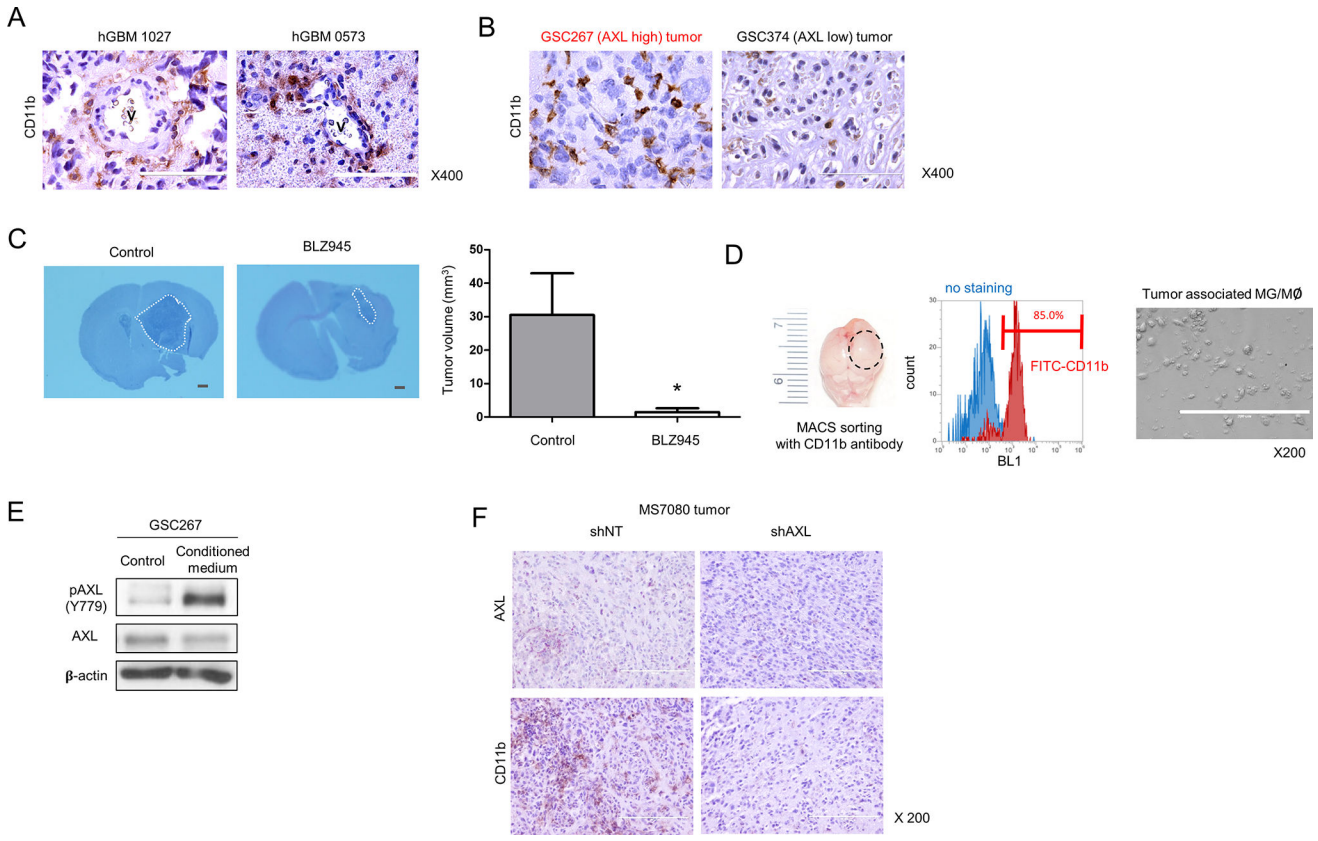

Figure 3.

Tumor-associated macrophages activate AXL in GSCs. **A.** IHC analysis of human GBMs using CD11b antibodies; vessels (V) are shown. Scale bars, 100 μm. **B.** IHC analysis of tumors from xenograft mice inoculated with either GCS267 (AXL high) or GSC374 (AXL low) cells using CD11b antibodies. Scale bars, 100 μm. **C.** CD11b(+) cell depletion by BLZ945, Csf1b inhibitor, suppresses tumor growth. H&E staining and tumor volume of a MS7080 tumor from mice treated with BLZ945 (* $P < 0.05$). White broken lines show the tumor area. Scale bars, 1 mm. **D.** After MACS sorting of xenograft samples with a CD11b antibody (left), data obtained from FACS analysis show that samples consist of more than 85% CD11b positive cells (middle). Ten thousand cells were cultured in 1 mL RPMI-1640 medium without serum for 48 hours (right). Scale bars, 200 μm. **E**. Western blot analysis of phospho (p) and total AXL in GSC267 cells starved for 24 h, followed by incubation with conditioned medium from CD11b-expressing cells (described in **C**). β-Actin served as a loading control. **F.** Representative images of IHC analysis using AXL or CD11b antibodies after the intracranial transplantation of MS7080 transduced with shRNA against AXL (shAXL) or a non-targeting control (shNT). Scale bars, 200 μm.

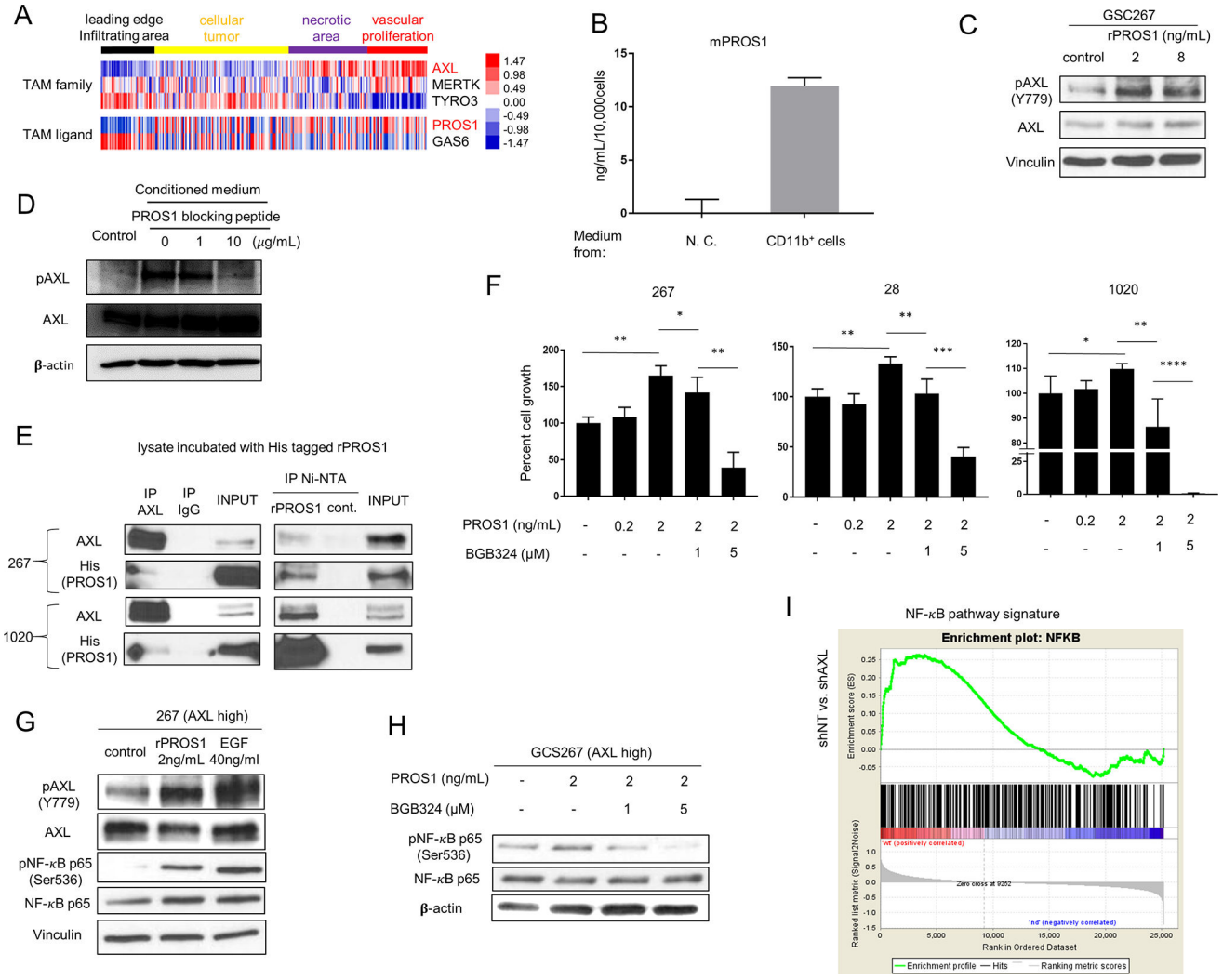

Figure 4.

PROS1 activates AXL in GSCs. **A.** Heat map obtained from the IVY Atlas Project database showing the localization differences between TAM receptors and ligands. **B.** ELISA of mouse PROS1 (mPROS1) expression in conditioned medium from tumor-associated MG/Mø or medium alone (no cells, “N.C.”). Ten thousand cells, enriched for CD11b expression (as in Fig. 3D), were cultured in 1 mL RPMI-1640 medium for 48 hours, and the supernatant was used for the ELISA. **C.** Western blot analysis of total and phospho-AXL in GSC267 cells treated with 2 or 8 ng/mL of recombinant PROS1. **D.** Western blot analysis of total- and pAXL in GSC267 cells starved for 24h, followed by incubation with conditioned medium treated with 1 or 10 μg/mL of PROS1 blocking peptide. **E.** Immunoprecipitation (IP) analysis of GSC lysates using an AXL antibody (left panel) or Ni-NTA for PROS1 (right panel), followed by immunoblot for PROS1 and AXL, showing the AXL-PROS1 interaction. Cells were harvested 24 h after EGF, bFGF, and B27 starvation; lysates were then incubated with His-tagged rPROS1. Whole cell lysates with input rPROS1 served as a positive control, and pull-downs with immunoglobin G served as a negative control. **F.** Cell growth assays for three different GSCs (28, 267, and 1020) expressing high AXL levels

treated with PROS1 and BGB324 for 24 h (* $P < 0.05$, ** $P < 0.01$, or *** $P < 0.001$). The cells were cultured in medium without EGF/bFGF and B27. **G.** Western blot analysis of total AXL, pAXL, and their downstream target, pNF-κB p65. Cells were starved of EGF/FGF and B27 for 24 h, then harvested after 30 min of treatment with 2 ng/mL PROS1 or 40 ng/mL EGF. Vinculin served as a loading control. **H.** Western blot analysis of pNF-κB p65 and total NF-κB after treatment with PROS1 with or without BGB324; cells were treated as above in (**F**). β-Actin served as a loading control. **I**. GSEA showing NF-κB signature is reduced in AXL-depleted GSCs. NES is shown in the plot.

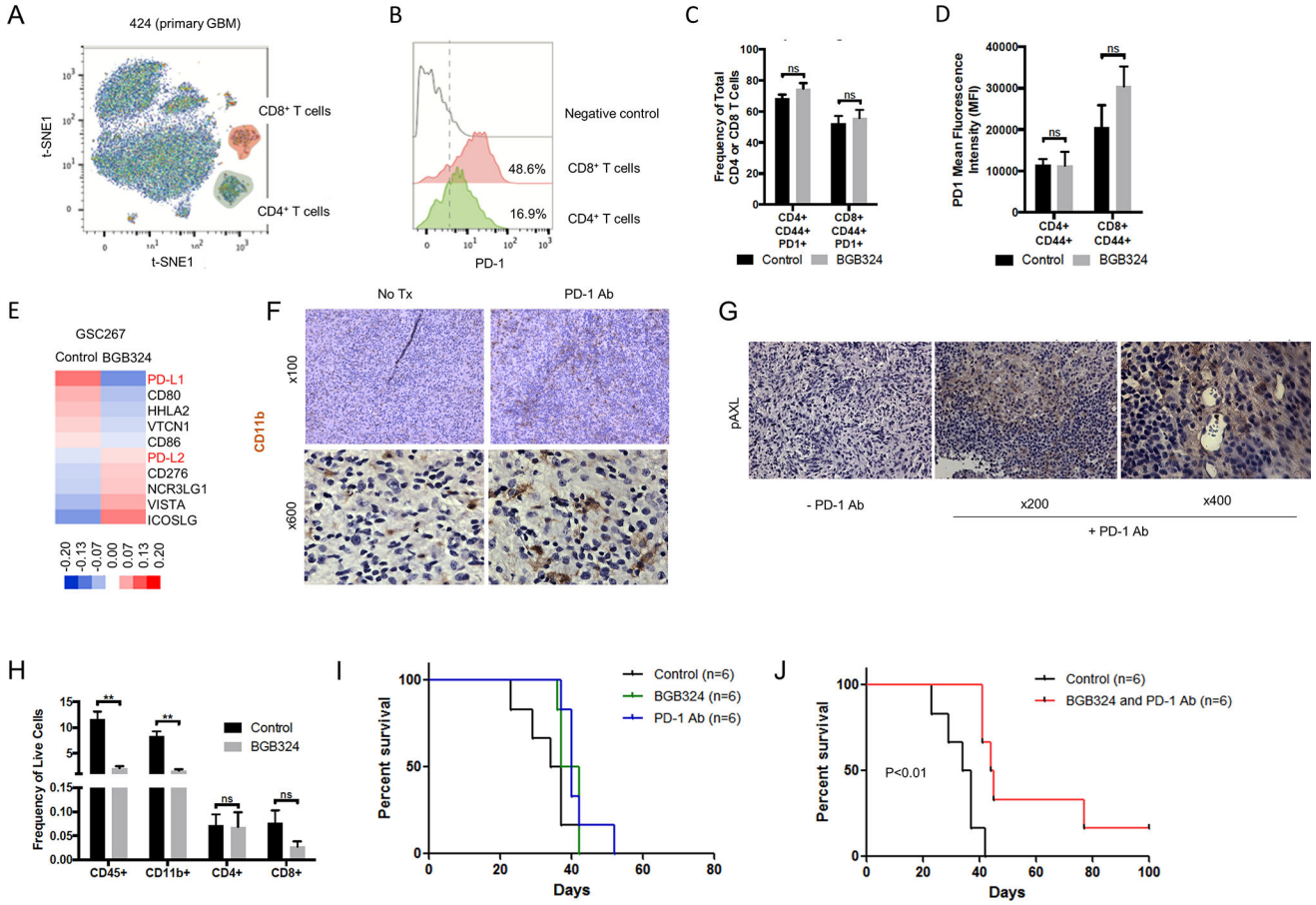

Figure 5.

Co-treatment with BGB324 and PD-1 antibodies improves survival in mouse GBM models. **A**. Detection of CD4 (CD45+ CD3+ CD8+ CD4+) and CD8 T (CD45+ CD3+ CD4− CD8+) cell from primary GBM dissociated cells (424) after selection of CD45+ selection by CyTOF. **B**. Detection of PD-1 in CD4 and CD8 T infiltrating cells primary GBM tumor (424). Negative control: naïve CD8 T cells from blood. **C–D.** Effect of BGB324 on activated intratumoral T cells expressing PD-1. (C) Frequency of total CD4(+) or CD8(+) T cells in mouse tumors from mice treated with BGB324 for 10 days (50 mg/kg/day). (D) mean fluorescence intensity (MFI). **E**. Heat map of the B7 family generated using microarray data obtained from GSC267 xenograft tumors treated with BGB324. **F.** IHC analysis showing CD11b staining in a representative sample of a MS7080 tumor from mice treated with PD-1 antibody (Ab). **G.** IHC analysis of mouse tumors from mice treated with PD-1 Ab using pAXL Ab. **H.** The frequency of infiltrating CD45(+), CD11b(+), CD4(+), or CD8(+) cells in mouse tumors from mice treated with BGB324. **F.** Kaplan-Meier curve of MS7080 tumor-bearing mice treated with PD-1 Ab four times (10 mg/kg, days 3, 7, 10 and 13) or BGB324 for 10 days (50 mg/kg/day). **G.** Kaplan-Meier curve for mice with MS7080 tumors treated with PD-1 Ab four times (10 mg/kg, days 3, 7, 10 and 13) and BGB324 for 10 days (50 mg/kg/day).

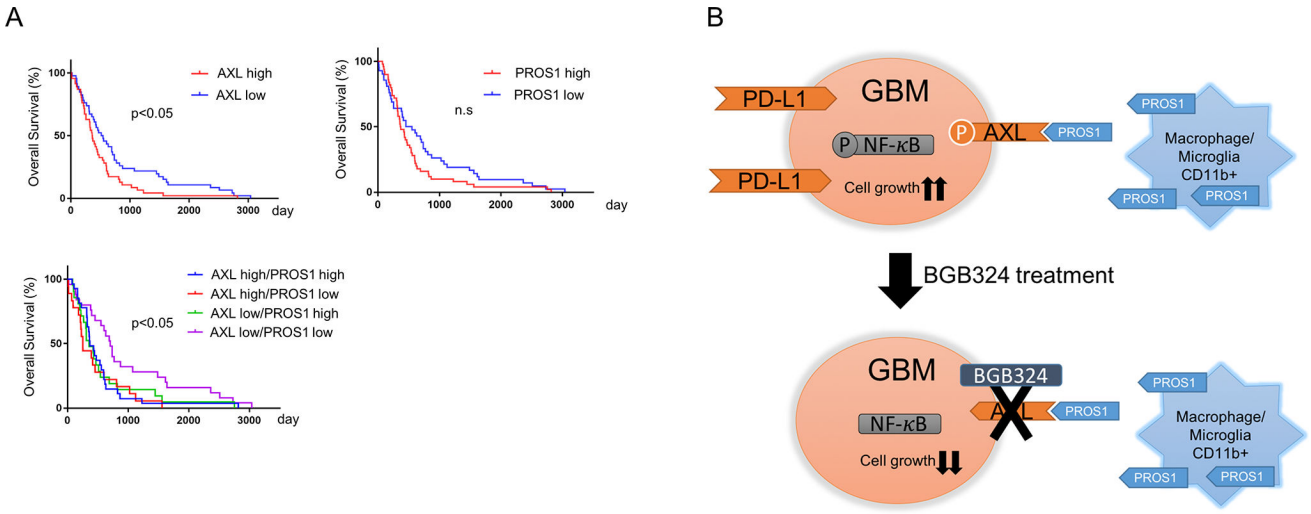

Figure 6.

Expression of either AXL and/or PROS1 were clinically associated with a poor prognosis for GBM patients. **A.** Kaplan-Meier curve showing patient survival data (TCGA data) stratified based on AXL and PROS1 expression levels. Patients expressing lower levels of AXL survived for a significantly longer period than those expressing higher levels (upper left). Patients expressing lower levels of PROS1 survived for a significantly longer period than those expressing higher levels (upper right). Patients expressing lower levels of both AXL and PROS1 survived longer than other groups (lower left). Statistical analysis was performed with a log-rank test ($P < 0.05$). **B.** Schematic representation of the effects of BGB324 treatment on GBM. Tumor-associated macrophages produce PROS1, which binds to AXL resulting in AXL phosphorylation and activation. Downstream targets of AXL, such as NF-κB, are activated, leading to expression of PD-L1 and subsequent cell growth. These events are inhibited by BGB324 treatment.